www.elsevier.nl/locate/jorganchem

Journal of Organometallic Chemistry 620 (2001) 243–248

Journal of Organometallic Chemistry

Study on structural properties and solution dynamics of zinc complexes with the (*N*,*N*-dimethylaminomethyl)ferrocenyl ligand

Naka Seidel [a], Klaus Jacob [a,*], Piero Zanello [b], Marco Fontani [b]

[a] *Institut für Anorganische Chemie der Martin-Luther-Universität Halle-Wittenberg, Geusaer Strasse 88, D-06217 Merseburg, Germany*
[b] *Dipartimento di Chimica dell'Università di Siena, Pian dei Mantellini 44, I-53100 Siena, Italy*

Received 29 August 2000; received in revised form 16 October 2000

Abstract

The reaction of {*C*,*N*-[Fe(η^5-C_5H_5)(η^5-C_5H_3(CH_2NMe_2)-2)]}Li, (FcN)Li, with zinc chloride affords the diorganozinc complex $(FcN)_2Zn$ (**1**). In solution, **1** appears as a mixture of rac and meso diastereomers, whereas in the solid state it crystallizes solely as a rac diastereomer. The ratio of rac/meso diastereomers in solution is solvent-, temperature- and concentration-dependent, consistent with an intermolecular exchange between diastereomers. An intramolecular dynamic phenomenon involving dissociation and recoordination of Zn–N bonds was also observed. The reaction of **1** with zinc chloride yields the monoorganozinc compound (FcN)ZnCl (**2**) as a slightly soluble yellow microcrystalline powder.

Keywords: Chelates; Chirality; Crystal structure; Cyclovoltammetry; *N*,*N*-Dimethylaminomethylferrocenyl; Zinc

1. Introduction

Recent studies on the complexation behavior of the *N*,*N*-dimethylaminomethylferrocenyl ligand (FcN) dealt with molecules in which the FcN ligand is either (*C*,*N*)-bidentate, *C*-monodentate, *C*-bridging or μ(*C*,*N*)-bridging [1]. Some of these compounds exchange between some of these bonding modes in solution, like $(FcN)_2Pb$ [2] and $(FcN)_2Mg$(solv) (solv = ether, THF) [3]. When two or more FcN ligands are coordinated in the same molecule the formation of diastereomers is possible, due to the chirality of the FcN ligand [4]. Owing to this stereochemical marker, we discovered an interesting intermolecular exchange phenomenon between rac and meso diastereomers for magnesium and lead compounds.

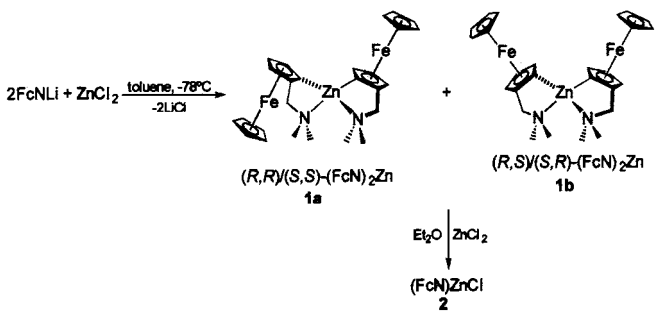

Scheme 1.

Initiated by known similarities of divalent states of magnesium and zinc with respect to coordination chemistry, we decided to study the analogous chemistry of FcN compounds of zinc. Another aspect of this research is the fact that the organozinc compounds are, just like those of magnesium, valuable precursors for the synthesis of other transition metal complexes. Therefore, it is important to elucidate their behavior in solution. Thiele and coworkers did some preliminary work, but general spectroscopic and structural data are lacking [5].

2. Results and discussion

The reaction of zinc chloride with two equivalents of (FcN)Li [6] in diethyl ether at room temperature yields a solution of **1** (Scheme 1). The ^{1}H- and ^{13}C-NMR data of **1** in toluene-d_8 at 23°C (after taking a sample and

* Corresponding author. Tel.: +49-3461-462068; fax: +49-3461-462002.
E-mail address: jacob@chemie.uni-halle.de (K. Jacob).

0022-328X/01/$ - see front matter
PII: S0022-328X(00)00781-6

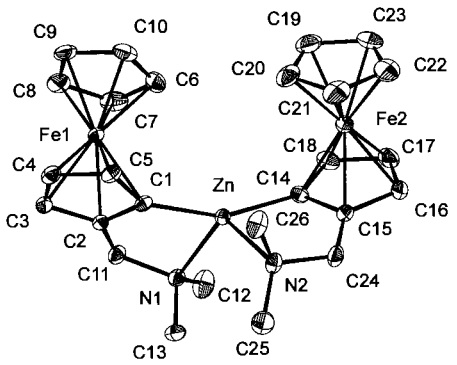

Fig. 1. Molecular structure of **1** ((*R*,*R*) diastereomer) with thermal ellipsoids at 50% probability level. H atoms are omitted for clarity.

Table 1
Selected molecular bond lengths (Å) and angles (°) in complex **1**. Estimated S.D. values are in parentheses

Zn–C1	1.948(2)	Fe1–C(1m)[a]	1.6511
Zn–C14	1.945(2)	Fe1–C(2m)	1.6493
Zn–N1	2.3091(16)	Fe2–C(3m)	1.6480
Zn–N2	2.3622(16)	Fe2–C(4m)	1.6435
C1–Zn–C14	155.54(8)	C2–C1–Zn	113.10(15)
N1–Zn–N2	115.25(6)	C15–C14–Zn	113.78(15)
C1–Zn–N1	82.02(7)	C5–C1–Zn	141.01(15)
C14–Zn–N2	83.06(8)	C18–C14–Zn	140.94(17)
Zn–N1–C11	105.04(11)	C11–N1–C12	111.09(18)
Zn–N1–C12	116.62(16)	C11–N1–C13	109.12(18)
Zn–N1–C13	103.85(14)	C12–N1–C13	110.6(2)
Zn–N2–C24	105.08(12)	C24–N2–C25	109.75(18)
Zn–N2–C25	123.06(16)	C24–N2–C26	110.98(19)
Zn–N2–C26	98.08(13)	C25–N2–C26	109.2(2)
N1–C11	1.480(2)	N2–C24	1.475(3)
N1–C12	1.457(3)	N2–C25	1.465(3)
N1–C13	1.461(3)	N2–C26	1.459(3)

[a] The suffix 'm' denotes the centroid of a Cp ring.

removal of ether in vacuo) show that $(FcN)_2Zn$ appears in solution as a mixture of diastereomers **1a** and **1b** respectively in a ratio of 4:1. After cooling the solution, only the major diastereomer **1a** crystallizes in the form of large orange prisms in 80% yield. The compound is moderately air stable in the solid state, but in solution it decomposes immediately when exposed to air. **1** is readily soluble in both polar and non-polar solvents.

X-ray diffraction analysis revealed that compound **1** crystallizes completely as a rac diastereomer. The diastereomer **1a** possesses a set of (*R*,*R*)-configured (or (*S*,*S*)) FcN ligands (rac diastereomer); therefore, it is assumed that in diastereomer **1b** one of the ligands is in the *R*-configuration and the other in the *S*-configuration (meso diastereomer). The molecular structure of **1a** is shown in Fig. 1; the most important molecular dimensions are summarized in Table 1.

The zinc atom exhibits an extremely distorted tetrahedral coordination and binds two (*C*,*N*)-chelate-bonded FcN ligands. The C1–Zn–C14 bond angle of 155.54(8)° and N1–Zn–N2 bond angle of 115.28(8)° illustrate the strong distortion of the molecule. They are comparable with the C–Zn–C bond angle of 156.48(2)° and the N–Zn–N angle of 109.7(1)° found in $[Me_2NCH_2CH_2CH_2]_2Zn$ [7].

The Zn–C1 and Zn–C14 bond lengths are 1.948(2) Å and 1.945(2) Å, respectively, which is slightly shorter than the average Zn–C bond length in $[Me_2NCH_2CH_2CH_2]_2Zn$ [7] of 1.9848(5) Å and the corresponding values found in $Zn[CH(SiMe_3)_2]_2$·bipy, (2.034(5) and 2.035(5) Å) [8]. The Zn–N1 and Zn–N2 bonds of 2.3091(16) and 2.3622 (16) Å are extremely long, which is to be expected owing to a strongly widened C–Zn–C bond angle [9]. These bonds differ significantly from each other and, therefore, might be interpreted as a remnant of the intramolecular dynamics present in solution (vide infra). The Zn–N1 bond is comparable to the average Zn–N bond lengths of 2.307(4) Å found in $[Me_2NCH_2CH_2CH_2]_2Zn$ [7]. The Zn–N bond lengths are also significantly longer than the Zn–N bonds in $[Zn(NH_3)_4]Cl_2$ of 2.03 Å [10], and those of 2.131 Å found in $Zn(en)_2Cl_2$ [11], and can be considered as labile bonds. Another example of a zinc compound having Zn in a two-carbon–two-nitrogen coordinate environment (albeit in a different chelate configuration) is provided by $Zn\{NC_5H_4C(SiMe_3)_2\text{-}2\}_2$ [12], in which the Zn–C distance is 2.07(0) Å and the Zn–N distance 2.29(4) Å, which is similar to bond distances found in **1**.

The average C–C bond lengths in ferrocene cyclopentadienyl rings are 1.424(8) Å and the average Fe–C(Cp) distance is 2.042(2) Å, which is very similar to ferrocene itself [13]. However, the Fe–C1 and Fe–C14 distances of 2.0823(19) Å and 2.1005(19) Å respectively are somewhat longer than the other bond lengths, reflecting the bonding of C1 and C14 to the zinc atom.

The small bite angle of the FcN ligands (C–Zn–N ca. 82°) causes distortions around the α-carbon atoms and nitrogen atoms. For instance, although the C–N–C angles have ideal values, the Zn–N1–C11 and Zn–N2–C24 angles (105.04(11)° and 105.08(12)° respectively) are smaller than the other Zn–N–C angles. Similarly, the C2–C1–Zn and C15–C14–Zn (113.10(15)° and 113.78(15)° respectively) are smaller than C5–C1–Zn and C18–C14–Zn angles (141.01(15)° and 140.94(17)° respectively). Such a small bite angle is a characteristic of FcN compounds, because similar values are found in $(FcN)_2Mg(OEt_2)$ (78.89(7) and 78.69(7)°) [3], $(FcN)_2Mg(THF)$ (78.07(8) and 78.60(8)°) [3] and $(FcN)_2Pb$ (71.5(1) and 71.3(1)° for $C2/c$ polymorph; 70.8(2) and 71.8(2)° for $P2_1/n$ polymorph) [2]. The difference depends solely on the radius of the coordinated metal; the larger the metal radius, the smaller the bite angle.

The ^{1}H- and ^{13}C-NMR data of **1** in both THF-d_8 and toluene-d_8 at room temperature show only one set of

signals for both FcN groups in each diastereomer (Table 2). At −80°C in THF-d_8 the signal of the methyl groups of the main diastereomer **1a** start to broaden. In toluene-d_8 the signal is already broadened at −40°C and at −80°C there are two signals at 1.71 and 2.35 ppm. The signals for the methylene groups appear as two doublets for the whole temperature range studied. The appearance of two methyl signals and two doublets for methylene protons indicates the equivalency of both FcN ligands and is consistent with the C_2 symmetry of the molecule. Therefore, it is concluded that the main diastereomer **1a** is indeed *rac*-$(FcN)_2Zn$. The signals of *meso*-$(FcN)_2Zn$ (**1b**) do not reach decoalescence at −80°C in either toluene-d_8 or THF-d_8. The temperature-dependent NMR data indicate intramolecular dynamics and can be explained by a rapid dissociation and recoordination of the Zn–N bonds.

The ratio of diastereomers measured in different solvents (THF-d_8, toluene-d_8) is temperature- and concentration-dependent (4.4 in THF-d_8 at 30°C (c_1 = 0.1 mol dm^{-3}), 4.9 in toluene-d_8 at 23°C (c_2 = 0.3 mol dm^{-3}) and 7.4 in toluene-d_8 at 18°C (c_3 = 0.1 mol dm^{-3})) and suggests an intermolecular exchange between diastereomers.

The data in THF-d_8 (c_1 = 0.1 mol dm^{-3}) show that the proportion of rac diastereomer is higher at lower temperatures. This observation is reminiscent of that for the magnesium compound $(FcN)_2Mg$ [3]. The equilibrium constant K (rac/meso) gradually changes from 4.1 at 30°C to 5.9 at −80°C. Plotting ln K against $1/T$ (Van't Hoff plot) gives a straight line from which the thermodynamic parameters $\Delta H = -1.7$ kJ mol^{-1} and $\Delta S = 6.3$ J mol^{-1} K^{-1} for c_1 were obtained ($r = 0.9948$) (Fig. 2). These parameters may be compared with those calculated for the sample of $(FcN)_2Mg$ with similar concentration ($\Delta H = -5.92$ kJ mol^{-1} and $\Delta S = -12.1$ J mol^{-1} K^{-1}) [3], indicating smaller temperature dependence in the case of zinc.

The rac/meso ratio of a saturated (c_2 = 0.3 mol dm^{-3}) and a diluted (c_3 = 0.1 mol dm^{-3}) sample in toluene-d_8 was monitored at different temperatures (Fig. 2). At room temperature *rac*-$(FcN)_2Zn$ prevails; by heating the samples to 60°C its proportion is lower, which is consistent with the observed behavior in THF-d_8. It can be seen that the proportion of *rac*-$(FcN)_2Zn$ in the diluted sample is higher than in the saturated sample for a measured temperature interval. The equilibrium constant K (rac/

Table 2
^{1}H-NMR data for **1** and **2**[a]

		NMe_2	CH_2N	CpFe	C_5H_3
30°C, THF-d_8	*rac*-**1**	2.42 (s, 12H)	3.13 (d, 2H, J = 15) 3.61 (d, 2H, J = 15)	4.08 (s, 10H)	4.14 (s, 2H) 4.24 (s, 4H)
	meso-**1**	2.46 (s, 12H)	3.12 (d, 2H, J = 14) 3.67 (d, 2H, J = 14)	4.02 (s, 10H)	3.96 (s, 2H) 4.07(s, 2H) 4.12 (s, 2H)
23°C, toluene-d_8	*rac*-**1**	2.28 (s, 12H)	3.07 (d, 2H, J = 15) 3.60 (d, 2H, J = 15)	4.33 (s, 10H)	4.29 (s, 2H) 4.34 (s, 2H) 4.56 (s, 2H)
	meso-**1**	2.37 (s, 12H)	3.08 (d, 2H, J = 14) 3.58 (d, 2H, J = 14)	4.32 (s, 10H)	4.22 (s, 2H) 4.39 (s, 2H) 4.51 (s, 2H)
−80°C, THF-d_8	*rac*-**1**	2.45 (s, br)	3.17 (d, 2H, J = 15) 3.56 (d, 2H, J = 15)	4.08 (s, 10H)	4.12 (s, br, 2H) 4.21 (s, br, 2H)[b]
	meso-**1**	–[b]	3.07 (d, 2H, J = 14) 3.61 (d, 2H, J = 14)	3.99 (s, 10H)	3.88 (s, br, 2H) 4.06 (s, br, 2H) 4.14 (s, br, 2H)
−80°C, toluene-d_8	*rac*-**1**	1.72 (s, br, 6H) 2.35 (s, br, 6H)	2.84 (d, 2H, J = 15) 3.02 (d, 2H, J = 15)	4.30 (s, 10H)	4.28 (s, 4H) 4.56 (s, 2H)[b]
	meso-**1**	–[b]	2.76 (d, 2H, J = 15) 3.19 (d, 2H, J = 15)	4.17 (s, 10H)	4.35 (s, 2H) 4.49 (s, 2H)[b]
25°C	**2**	2.15 (s, 6H)	3.23 (d, 1H, J = 12) 4.00 (d, 1H, J = 12)	4.23 (s, 5H)	4.20 (s, 1H) 4.45 (s, 1H) 4.50 (s, 1H)
−30°C	**2**	2.08 (s, 3H) 2.21 (s, 3H)	3.23(d, 1H, J = 12) 4.00 (d, 1H, J = 12)	4.22 (s, 5H)	4.21 (s, 1H) 4.46 (s, 1H) 4.50 (s, 1H)

[a] The spectra of **1** measured in THF-d_8 and toluene-d_8, **2** in pyridine-d_5.
[b] Not all signals were observed, due to overlapping with other signals.

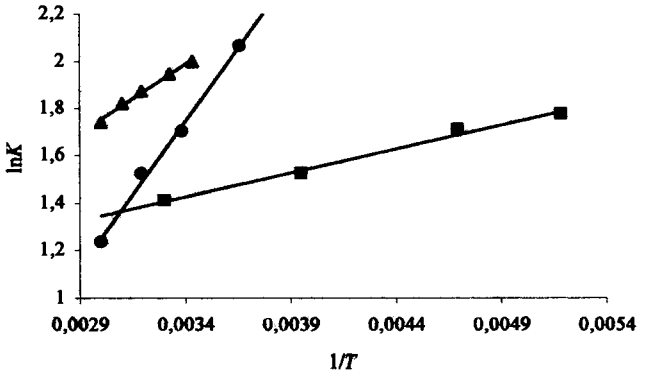

Fig. 2. Van't Hoff plots for **1** in THF-d_8 and toluene-d_8. (K = *rac*-$(FcN)_2Zn$/*meso*-$(FcN)_2Zn$). Legend: (●) $c_2 = 0.1$ mol/l in toluene-d_8, (■) $c_3 = 0.3$ mol/l in toluene-d_8, (▲) $c_1 = 0.1$ mol/l in THF-d_8.

meso) gradually changes from 7.9 at 0°C to 3.4 at 60°C for c_2 and from 7.1 at 18°C to 5.7 at 60°C for c_3. By lowering the temperature below 0°C it was observed that the sample became turbid and the material precipitated from the solution; therefore, no further measurements were done. Plotting ln K against $1/T$ (Van't Hoff plot) for each concentration (c_2 and c_3) gives straight lines from which the thermodynamic parameters $\Delta H = -10.3$ (c_2) and -4.9 kJ mol^{-1} (c_3) and $\Delta S = -20.4$ (c_2) and -0.03 J mol^{-1} K^{-1} (c_3) were obtained ($r = 0.9971$ and 0.9937 for c_2 and c_3 respectively). As expected, the slope of the Van't Hoff curve is smaller for c_3 than c_2, as the probability for an intermolecular exchange process is lower at lower concentrations. Therefore, the rac/meso equilibrium is less temperature-dependent than for higher concentrations.

The mechanistic pathway for the observed intermolecular exchange most likely involves electron-deficient three-center two-electron interactions (see Scheme 2). It invokes a concerted intermolecular migration of two σ-bonded FcN groups through an intermediate with carbon-bridged FcN groups. This mechanism is virtually identical to that proposed for $(FcN)_2Mg$ [3], but it differs from that proposed for $(FcN)_2Pb$ [2] in that exchange of FcN ligands seems to be preceded by a Pb–Pb interaction. The similar pathways for zinc and magnesium compounds are to be expected owing to the similar chemical behavior of the metals.

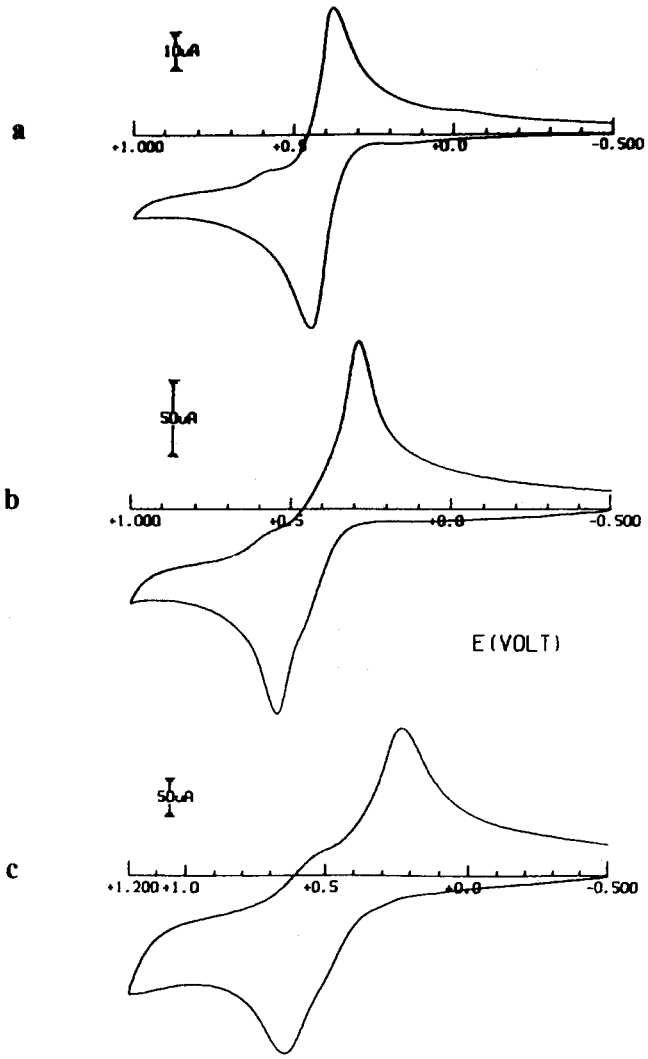

Fig. 3. Cyclic voltammograms recorded at a platinum electrode in CH_2Cl_2 solution containing **1** (1.8×10^{-3} mol dm^{-3}) and $[NBu_4][PF_6]$ (0.2 mol dm^{-3}). Scan rates: (a) 0.05 V s^{-1}; (b) 0.5 V s^{-1}; (c) 2.00 V s^{-1}.

The redox behavior of **1** was examined by electrochemical techniques (Fig. 3). At a low scan rate it undergoes a single-stepped two-electron oxidation (proved by controlled-potential coulometry at $+0.8$ V) at $E^{\circ\prime} = +0.43$ V that has features of transient chemical reversibility (at 0.05 V s^{-1}: $i_{pc}/i_{pa} = 0.8$; $\Delta E_p =$ 68 mV). A progressive increase of the scan rate (Fig.

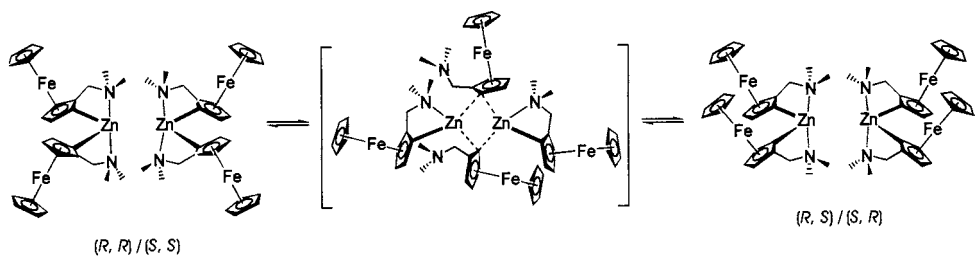

Scheme 2.

3a–c) causes splitting of the oxidation process into two separate anodic steps (at approximately $E^{\circ\prime} = +0.37$ and $+0.57$ V). The occurrence of adsorption phenomena can be discarded, in that the anodic peak current increases linearly with the square root of the scan rate. In agreement with this picture, cyclic voltammetric tests performed upon the progressive two-electron oxidation in macroelectrolysis reveal at intermediate times the appearance of two new reversible systems at $E^{\circ\prime} = +0.35$ and $+0.54$ V; then any peak system completely disappears. At the same time, the initially yellow solution changes to a green–gray color, indicating the decomposition of **1**. It is assumed that formation of FcNH ($E^{\circ\prime} = +0.38$ V) is an intermediate step in the degradation pathway.

The ligand distribution between $(FcN)_2Zn$ and $ZnCl_2$ gave the monoorganozinc complex (FcN)ZnCl (**2**). As for the equivalent magnesium compound (FcN)MgX [3], **2** cannot be obtained by a direct 1:1 reaction of $ZnCl_2$ and (FcN)Li. Compound **2**, m.p. 160°C, precipitated as a yellow powder that could not be induced to crystallize. It is insoluble in non-polar solvents (pentane), only slightly soluble in polar solvents (ether, THF) and soluble in pyridine. **2** was characterized by ^{1}H- and ^{13}C-NMR spectroscopy and mass spectroscopy ($m/z = 341$ at 70 eV). ^{1}H- and ^{13}C-NMR data of **2** at room temperature in pyridine-d_5 show that the methylene protons are magnetically non-equivalent, but only one *N*-methyl resonance is observed. At -30°C the methyl signal splits in two singlets at 2.08 and 2.21 ppm, indicating the intramolecular dynamics caused by dissociation and recoordination of Zn–N bonds, as found for **1**.

3. Conclusions

Organozinc compounds **1** and **2** are both highly dynamic in solution. Although compound **1** crystallizes solely as the (*C*,*N*)-bonded rac diastereomer, a mixture of meso and rac diastereomers forms in solution. The rac/meso ratio is solvent-, temperature- and concentration-dependent, consistent with an intermolecular exchange between diastereomers. In general, the proportion of *rac*-$(FcN)_2Zn$ is higher at lower temperatures. An intramolecular dynamic process of dissociation and recoordination of Zn–N bonds is observed for both **1** and **2**. For the organozinc compounds the behavior observed is similar to that of the magnesium compounds, owing to the similar chemical properties of the metals.

4. Experimental

4.1. General procedures

All manipulations were carried out by using standard Schlenk techniques under an inert argon atmosphere. All solvents were dried by standard procedures and distilled under argon prior to use. (FcN)Li was prepared by a previously described method [6]. $ZnCl_2$ was purchased commercially and used as received. Pyridine-d_5 was dried by distillation from CaH_2. ^{1}H- and ^{13}C-NMR data were recorded on a Varian 300 MHz and 500 MHz instrument and referenced to the deuterated solvent. Mass spectra were recorded on an AMD 402 by EI at 70 eV; m/z values refer to ^{35}Cl and ^{64}Zn.

Materials and apparatus for electrochemistry have been described elsewhere (three-electrode cell, platinum disk as a working electrode, platinum spiral as a counterelectrode) [14]. All potential values are referred to the saturated calomel electrode (SCE). Under the present experimental conditions (dichloromethane solution containing $[NBu_4][PF_6]$ as a supporting electrolyte (0.2 mol dm^{-3}) the one-electron oxidation of ferrocene occurs at $E^{\circ\prime} = +0.38$ V.

4.2. Synthesis of $(FcN)_2Zn$ (1)

A solution of (FcN)Li (5.92 g, 23.8 mmol) in diethyl ether (50 ml) was added to a rapidly stirred solution of $ZnCl_2$ (1.62 g, 11.9 mmol) in diethyl ether (50 ml) with cooling to ca. -78°C. The reaction mixture became an orange color and was stirred for 1 h and then allowed to warm up to room temperature (r.t.). After stirring for 24 h the diethyl ether was removed under reduced pressure, and the orange residue extracted with toluene (30 ml). After filtering, the orange solution was reduced to incipient crystallization and stored at -30°C to give orange crystals. Yield: 0.52 g, 80%. M.p. 113°C. Anal.

Table 3
Crystallographic data for **1**

Empirical formula	$C_{26}H_{32}Fe_2N_2Zn$
Molecular mass	549.61
Crystal dimensions (mm^3)	$0.80 \times 0.50 \times 0.40$
Crystal system	monoclinic
Space group	$P2_1/c$
a (Å)	11.2622(15)
b (Å)	11.857(2)
c (Å)	18.469(3)
β (°)	104.77(3)
V (Å^3)	2384.7(6)
Z	4
d_{calcd} (g cm^{-3})	1.531
T (K)	173(2)
μ (mm^{-1})	2.214
θ_{max} (°)	26.1
No. of reflections	18693
No. of unique reflections	4652
Structure determination	Direct methods
Refinement	on F^2 in SHELXL
No. of parameters	408
$R_1[I > 2\sigma(I)]$	0.0264
wR_2 (all data)	0.0670
Goodness-of-fit (on F^2)	1.034

Found: C, 56.35; H, 5.78; N, 5.06. Calc. for $C_{26}H_{32}Fe_2N_2Zn$: C, 56.81; H, 5.87; N, 5.10%. $^{13}C\{^1H\}$-NMR data for **1a** (for **1b** in brackets): (toluene-d_8, r.t.) δ 47.1 [46.5] (NMe_2), 61.6 [62.2] (CH_2N), 68.8 [68.4] (C_5H_5), 71.6 [68.1] (C_5H_3), 73.7 [70.4] (C_5H_3), 74.3 [74.9] (C_5H_3–CH_2NMe_2), 95.8 [95.0] (C_5H_3–Zn).

4.3. Synthesis of (FcN)ZnCl (*2*)

A solution of **1** (3.11 g, 5.6 mmol) in diethyl ether (50 ml) was added to a rapidly stirred solution of $ZnCl_2$ (0.76 g, 5.6 mmol) in diethyl ether (50 ml) with cooling to ca. −78°C. The reaction mixture became a yellow color and was stirred for 1 h before being allowed to warm up to r.t. After removing the solvent under reduced pressure and filtration, the yellow residue was extracted with pentane to give a yellow microcrystalline powder. Yield: 1.53 g, 80%. M.p. 160°C (dec.). Anal. Found: C, 44.02; H, 4.76; Cl, 10.62; N, 3.72. Calc. for $C_{13}H_{16}ClFeZn$: C, 45.53; H, 4.70; Cl, 10.34; N, 4.08%. $^{13}C\{^1H\}$-NMR data for **2**: (pyridine-d_5, r.t.) δ 45.1 (NMe_2), 62.2 (CH_2N), 69.0 (C_5H_5), 70.7 (C_5H_3), 72.8 (C_5H_3), 77.4 (C_5H_3), 84.4 (C_5H_3–CH_2NMe_2), 92.6 (C_5H_3–Zn). MS m/z (%): 341 (M^+, 49).

4.4. X-ray structure analysis of *1*

Crystal and numerical data of the structure determination are given in Table 3. A single crystal was covered with inert oil and mounted on a glass fiber, and then transferred to the diffractometer in a stream of a cold gas (Stoe STADI IV-Diffractometer). Monochromatic Mo–K_α radiation ($\lambda = 71.073$ pm) was used. Data were corrected for Lorentz and polarization effects. The structures were solved by direct methods using the SHELXS program and refined by full-matrix least-squares against F^2 with SHELXL-97 [15]. All non-hydrogen atoms were refined with anisotropic thermal parameters. All hydrogen atoms were found in the difference Fourier map and refined isotropically.

5. Supplementary material

Crystallographic data (excluding structure factors) for the reported structure have been deposited with the Cambridge Crystallographic Data Centre as supplementary publication no. CCDC 114066. Copies of data can be obtained free of charge on application to The Director, CCDC, 12 Union Road, Cambridge CB2 1EZ, UK (fax: +44-1223-336093; e-mail: deposit@ccdc.cam.ac.uk).

Acknowledgements

N.S. thanks Dr A.A.H. van der Zeijden and Professor Dr D. Steinborn for fruitful discussions. The authors thank Professor Dr K. Merzweiler and Dr C. Wagner from the Institut für Anorganische Chemie der Martin-Luther-Universität Halle-Wittenberg for X-ray diffraction analysis. K.J. thanks the Deutsche Forschungsgemeinschaft DFG for financial support, N.S. thanks the DFG program 'Graduierten-Kolleg: Synthese und Reaktionsverhalten von Organometallverbindungen und Metallkomplexen' for a fellowship. P.Z. thanks the University of Siena for financial support (ex-quota 60%) and G. Montomoli for technical assistance.

References

[1] (a) K. Jacob, F.T. Edelmann, J. Prakt. Chem. 340 (1998) 393 and references cited therein. (b) P.B. Hitchcock, D.L. Hughes, G.J. Leigh, J.R. Sanders, J.S. de Souza, J. Chem. Soc. Dalton Trans. (1999) 1161.
[2] N. Seidel, K. Jacob, A.A.H. van der Zeijden, H. Menge, K. Merzweiler, C. Wagner, Organometallics 19 (2000) 1438.
[3] N. Seidel, K. Jacob, A.K. Fischer, C. Pietzsch, P. Zanello, Eur. J. Inorg. Chem. in press.
[4] K. Schlögl, M. Fried, Monatsh. Chem. 95 (1964) 558.
[5] C. Krüger, K.-H. Thiele, M. Dargatz, T. Bartik, J. Organomet. Chem. 362 (1989) 147.
[6] M.D. Rausch, G.A. Moser, C.F. Maede, J. Organomet. Chem. 51 (1973) 1.
[7] J. Dekker, J. Boersma, L. Ferholdt, A. Haaland, A. Spek, Organometallics 6 (1987) 1202.
[8] M. Westerhausen, B. Rademacher, W. Poll, J. Organomet. Chem. 421 (1991) 175.
[9] (a) M. Westerhausen, B. Rademacher, W. Schwarz, J. Organomet. Chem. 427 (1992) 275. (b) M. Westerhausen, M. Wieneke, W. Schwarz, J. Organomet. Chem. 522 (1996) 137.
[10] T. Yamagughi, H. Ohtaki, Bull. Chem. Soc. Jpn. 51 (1978) 3227.
[11] T. Fujita, T. Yamagughi, H. Ohtaki, Bull. Chem. Soc. Jpn. 52 (1979) 3539.
[12] M.J. Henderson, R.I. Papasergio, C.L. Raston, A.H. White, M.F. Lappert, J. Chem. Soc. Chem. Commun. (1986) 672.
[13] A. Haaland, J.E. Nilsson, Acta Chem. Scand. 22 (1968) 2653.
[14] A. Togni, M. Hobi, G. Rihs, G. Rist, A. Albinati, P. Zanello, D. Zech, H. Keller, Organometallics 13 (1994) 1224.
[15] (a) G.M. Sheldrick, SHELXS, Program for Crystal Structure Determination, University of Göttingen, Germany, 1986. (b) G.M. Sheldrick, SHELXL-97, Program for Crystal Structure Refinement, University of Göttingen, Germany, 1997.